PHYSICAL REVIEW B **96**, 020505(R) (2017)

Polarization-resolved terahertz third-harmonic generation in a single-crystal superconductor NbN: Dominance of the Higgs mode beyond the BCS approximation

Ryusuke Matsunaga,[1,2] Naoto Tsuji,[3] Kazumasa Makise,[4] Hirotaka Terai,[4] Hideo Aoki,[1,5] and Ryo Shimano[1,6]

[1]*Department of Physics, The University of Tokyo, Hongo, Tokyo 113-0033, Japan*

[2]*PRESTO, Japan Science and Technology Agency, 4-1-8 Honcho Kawaguchi, Saitama 332-0012, Japan*

[3]*RIKEN Center for Emergent Matter Science, Wako, Saitama 351-0198, Japan*

[4]*National Institute of Information and Communications Technology, 588-2 Iwaoka, Kobe 651-2492, Japan*

[5]*Electronics and Photonics Research Institute, Advanced Industrial Science and Technology, Umezono, Tsukuba, Ibaraki 305-8568, Japan*

[6]*Cryogenic Research Center, The University of Tokyo, Yayoi, Tokyo 113-0032, Japan*

(Received 9 March 2017; published 21 July 2017)

Recent advances in time-domain terahertz (THz) spectroscopy have unveiled that resonantly enhanced strong THz third-harmonic generation (THG) mediated by the collective Higgs amplitude mode occurs in s-wave superconductors, where charge-density fluctuations (CDFs) have been shown to also contribute to the nonlinear third-order susceptibility. It has been theoretically proposed that the nonlinear responses of Higgs and CDF exhibit essentially different polarization dependences. Here we experimentally discriminate the two contributions by polarization-resolved intense THz transmission spectroscopy for a single-crystal NbN film. The result shows that the resonant THG in the transmitted light always appears in the polarization parallel to that of the incident light with no appreciable polarization-angle dependence relative to the crystal axis. When we compare this with the theoretical calculation here with the BCS approximation and the dynamical mean-field theory for a model of NbN constructed from first principles, the experimental result strongly indicates that the Higgs mode rather than the CDF dominates the THG resonance in NbN. A possible mechanism for this is the retardation effect in the phonon-mediated pairing interaction beyond BCS.

DOI: 10.1103/PhysRevB.96.020505

Introduction. Spontaneous symmetry breakdown in many-body systems has been one of the central interests in condensed matter physics. Collective excitations arising from fluctuations of amplitude and phase of an order parameter are particularly intriguing as an inherent manifestation of a symmetry breaking, which have recently attracted renewed interests [1,2] since experimental techniques for accessing these modes were developed with ultrafast spectroscopy [3–6] or artificial control of physical parameters in the vicinity of quantum critical points [7–10]. Especially, the amplitude mode of the order parameter in superconductors has a close analogy with the Higgs boson in particle physics [11,12], hence called the Higgs amplitude mode [1].

The Higgs mode in superconductors has been identified with a Raman spectroscopy in $NbSe_2$, where a coexisting charge-density wave makes the mode Raman active [13–17]. For ordinary superconductors, however, the Higgs mode has eluded experimental detection until recently [18–20], primarily because the Higgs mode does not couple to electromagnetic fields in the linear-response regime [21]. Recently, a Higgs-mode oscillation with the superconducting gap frequency 2Δ was directly observed in a conventional s-wave superconductor $Nb_{1-x}Ti_xN$ by a terahertz (THz) pump-THz probe experiment [18] as the oscillation of order parameter in time domain after a nonadiabatic excitation [22–28]. Subsequently, it was revealed that irradiation of an intense narrow-band THz wave onto NbN with the photon energy ω tuned below 2Δ induces a third-harmonic generation (THG) [19]. A salient feature is that the THG intensity is strongly enhanced when the incident frequency doubled, 2ω, coincides with the gap, 2Δ. While THG from superconductors has been discussed phenomenologically in terms of a nonlinear supercurrent model [29], the resonant enhancement of the THG at $2\omega = 2\Delta$ has revealed the existence of a *nonlinear coupling* between the Higgs mode and electromagnetic wave [24,30]. Such a nonlinear THz spectroscopy provides a new tool for studying the collective modes which are now being theoretically studied for other types of exotic superconductors, *e.g.*, multiband [31–34] or d-wave superconductors [35].

Importantly, it has been pointed out that in addition to the Higgs mode, the charge-density fluctuation (CDF) or pair breaking, which has conventionally been identified as the origin of the peak at 2Δ in Raman spectroscopy [36], also induces the THG with a similar resonant character at $2\omega = 2\Delta$ [37]. Within the BCS mean-field approximation the CDF contribution is shown to be typically much larger than the Higgs-mode contribution [37]. However, their relative magnitudes should depend sensitively on how we take account of the many-body interactions. Indeed, a recent calculation with the dynamical mean-field theory (DMFT) has revealed that the BCS approximation significantly underestimates the Higgs-mode contribution because some of the important diagrams for the nonlinear optical susceptibility accidentally vanish in the BCS framework [38]. If we take account of dynamical correlations such as the retarded electron-phonon coupling or impurity scattering, the contribution of the Higgs mode to the THG is shown to be significantly enhanced and can even exceed the CDF [38]. NbN is in fact a strongly electron-phonon-coupled system with the dimensionless coupling constant $\lambda \sim 1$ [39–41], for which the retardation effect can invalidate the weak-coupling BCS treatment. It is thus imperative to decompose the Higgs and CDF contributions by experiments. One promising key is the dependence of the nonlinear susceptibility on the direction of the electric field

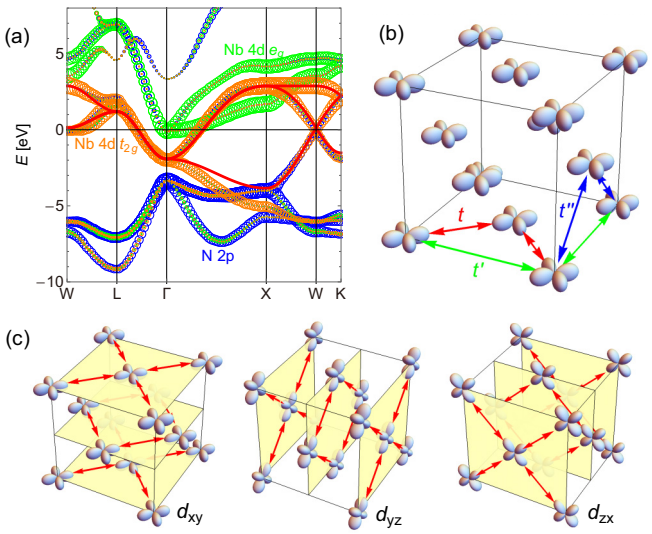

FIG. 1. (a) Band structure of NbN obtained from a first-principles calculation with the weights of the band character of Nb 4d e_g, 4d t_{2g}, and N $2p$ displayed in green, orange, and blue, respectively. Red curves represent the bands in the effective three-orbital model. (b) Nb $4d_{xy}$ orbitals on the fcc lattice. The arrows represent the hoppings with amplitudes t, t', and t''. (c) Sets of two-dimensional square lattices made of d_{xy}, d_{yz}, and d_{zx} orbitals respectively on xy, yz, and zx planes with a rotation of 45° on each plane.

polarization of the laser with respect to crystal axes of a superconductor, as discussed for a square lattice in Ref. [37].

The purpose of this paper is to discriminate the Higgs and CDF contributions from the polarization dependence of the nonlinear THG response for a conventional superconductor NbN. We theoretically evaluate the contributions to the THG with the BCS approximation and DMFT for a three-orbital model of NbN constructed from first principles. We shall show that the CDF contribution to THG increases by a factor of 2.3–2.7 when the polarization angle changes from [100] to [110]. We also find that the CDF contains a component for the polarization perpendicular to the incident field polarization. The Higgs contribution, by contrast, always arises parallel to the incident one with no angle dependence, as generally proved by a symmetry argument. Experimentally, we shall show in a polarization-resolved intense THz transmission spectroscopy for a single-crystal NbN film that the THG polarization is indeed parallel to the incident field and that the THG intensity hardly changes against the crystal axis orientation. From these theoretical and experimental results, we shall conclude that the Higgs mode plays a dominant role in the resonant enhancement of THG around $2\omega = 2\Delta$ in NbN.

Theoretical analysis. We construct an effective low-energy model of NbN based on a first-principles density-functional calculation using the WIEN2K package [42]. In Fig. 1(a) we display the band structure of NbN, which agrees with the previous results [43–45]. There are three bands around the Fermi energy ($E = 0$), which are mainly composed of $4d$ t_{2g} orbitals (d_{xy}, d_{yz}, and d_{zx}) of Nb. We illustrate $4d_{xy}$ orbitals on the fcc lattice in Fig. 1(b). The neighboring bands coming from Nb $4d$ e_g and N $2p$ orbitals are well separated from the t_{2g} bands in energy by a few electronvolts [Fig. 1(a)], which enables us to build an effective three-band tight-binding model in terms of the t_{2g} orbitals. For each orbital we take three hopping processes with amplitudes t, t', and t'' as displayed in Fig. 1(b). Since different t_{2g} orbitals at neighboring sites are orthogonal to each other, interorbital hoppings are suppressed. The resulting Hamiltonian reads

$$H_0 = \sum_{\boldsymbol{k},a,\sigma} \varepsilon_a(\boldsymbol{k}) d^\dagger_{a,\sigma}(\boldsymbol{k}) d_{a,\sigma}(\boldsymbol{k}),$$

where $a = xy$, yz, zx labels the orbitals, $d^\dagger_{a,\sigma}(\boldsymbol{k})$ creates a d electron with orbital a, spin σ, and momentum $\boldsymbol{k}$, and

$$\varepsilon_{xy}(\boldsymbol{k}) = 4t \cos\frac{k_x}{2}\cos\frac{k_y}{2} + 2t'(\cos k_x + \cos k_y) + 4t''\left(\cos\frac{k_y}{2}\cos\frac{k_z}{2} + \cos\frac{k_z}{2}\cos\frac{k_x}{2}\right),$$

with $\varepsilon_{yz}(\boldsymbol{k})$ and $\varepsilon_{zx}(\boldsymbol{k})$ given by permuting x, y, z. We fit the band dispersion to the result of the first-principles calculation to obtain the hopping parameters as $t = -0.72$ eV, $t' = -0.15$ eV, $t'' = 0.12$ eV, and the chemical potential $\mu = -0.6$ eV. The band dispersion of the effective model, plotted as a red curve in Fig. 1(a), shows that the t_{2g} bands are well reproduced by the effective model around the Fermi energy.

The polarization dependence of the THG is evaluated in the BCS approximation and in the DMFT. For the BCS, we take the pairing interaction,

$$H_{\rm int} = -\frac{1}{N}\sum_{\boldsymbol{k},\boldsymbol{k}',abcd} v_{ad,cb}(\boldsymbol{k},\boldsymbol{k}') d^\dagger_{a\uparrow}(\boldsymbol{k}) d^\dagger_{b\downarrow}(-\boldsymbol{k}) \times d_{c\downarrow}(-\boldsymbol{k}') d_{d\uparrow}(\boldsymbol{k}'),$$

where N is the number of k points and $v_{ad,cb}(\boldsymbol{k},\boldsymbol{k}')$ is the scattering matrix element, which can be expanded in each sector of irreducible representations Γ of the point group (O_h) for NbN as $v_{ad,cb}(\boldsymbol{k},\boldsymbol{k}') = \sum_\Gamma \sum_i v^\Gamma [\hat\varphi^\Gamma_i(\boldsymbol{k})]_{ab} [\hat\varphi^\Gamma_i(\boldsymbol{k}')]^*_{dc}$. Here v^Γ is the interaction parameter for sector Γ, with $\hat\varphi^\Gamma_i(\boldsymbol{k})$ being its ith basis function. We assume that the superconducting pairing realized in NbN belongs to the spin-singlet and orbital A_{1g} representation (with $[\hat\varphi^\Gamma_i(\boldsymbol{k})]_{ab} \propto \delta_{ab}$) and neglect the effect of the pairing interactions other than the A_{1g} sector. To reproduce the experimental condition for NbN, we take the model parameters for the superconducting gap $\Delta = 2.7$ meV $= 0.65$ THz and the temperature $T = 4$ K $= 0.34$ meV. In DMFT, we consider a three-orbital Holstein model,

$$H = \sum_{\boldsymbol{k},a,\sigma} \varepsilon_a(\boldsymbol{k}) d^\dagger_{a,\sigma}(\boldsymbol{k}) d_{a,\sigma}(\boldsymbol{k}) + \omega_0 \sum_i a^\dagger_i a_i + g\sum_{i,a}(a^\dagger_i + a_i)(n_{ia} - \langle n_{ia}\rangle),$$

where $a^\dagger_i$ creates a phonon at site i with frequency ω_0, g is the electron-phonon coupling, and $n_{ia} = \sum_\sigma d^\dagger_{ia\sigma} d_{ia\sigma}$ is the density of electrons. The impurity problem for DMFT is solved by the (unrenormalized) Migdal approximation with the effective pairing interaction projected to the orbital A_{1g} channel. The parameters are taken to be $\omega_0 = 0.5$ eV, $g = 3.0$ eV, and $T = 0.05$ eV as an example. We have confirmed that the results do not qualitatively change as the parameters

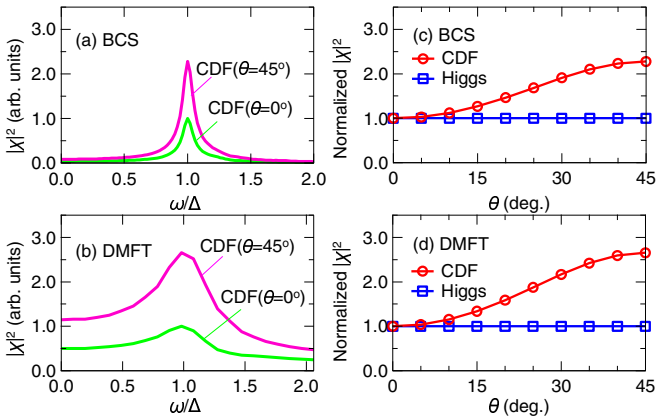

FIG. 2. (a, b) The CDF contribution to the THG intensity spectra $|\chi(\omega)|^2$ with $\boldsymbol{e}^I = \boldsymbol{e}^O = \boldsymbol{e}_\theta$ for $\theta = 0^\circ$ (lower curve) and 45° (upper) calculated in the BCS approximation (a) and DMFT (b). (c, d) The polarization dependence of the CDF and Higgs-mode contributions to the THG intensity $|\chi(\omega)|^2$ at resonance ($2\omega = 2\Delta$) with $\boldsymbol{e}^I = \boldsymbol{e}^O = \boldsymbol{e}_\theta$ calculated in the BCS approximation (c) and DMFT (d). The intensity in each panel is normalized by the value at $\theta = 0^\circ$. For the BCS approximation we take $\Delta = 2.7\,\text{meV} = 0.65\,\text{THz}$ and $T = 4\,\text{K}$ and for DMFT we take the Holstein model with $\omega_0 = 0.5\,\text{eV}$, $g = 3.0\,\text{eV}$, and $T = 0.05\,\text{eV}$.

are varied. The method for the calculation of the THG susceptibility is summarized in Supplemental Material [46]. We set the polarization $\boldsymbol{e}^I$ of the incident light and the polarization $\boldsymbol{e}^O$ along which the transmitted light is probed to be $\boldsymbol{e}^I = \boldsymbol{e}^O = \boldsymbol{e}_\theta = (\cos\theta,\ \sin\theta,\ 0)$.

We plot the BCS and DMFT results for the THG intensity $|\chi(\omega)|^2$ for $\theta = 0^\circ$ and 45° in Figs. 2(a) and 2(b). One can see that the CDF contribution has a resonance at $2\omega = 2\Delta$ for each θ. The intensities of the CDF at the resonance, $|\chi(2\omega = 2\Delta)|^2$, normalized by the value at $\theta = 0^\circ$, are plotted against θ in Figs. 2(c) and 2(d). Un-normalized plots showing the relative magnitudes are displayed in the Supplemental Material [46]. The CDF contribution has a characteristic polarization dependence with its intensity increasing by a factor of 2.3 (2.7) as θ is varied from 0° to 45° in the BCS (DMFT) result. On the other hand, the intensity of the Higgs-mode contribution does not depend on θ [Figs. 2(c) and 2(d)]. Although the relative magnitude between the CDF and Higgs is quite different between the BCS and DMFT results [38,46], the polarization dependence of the THG is qualitatively similar between the BCS and DMFT. The polarization dependence of the CDF can be qualitatively understood as follows: If we neglect the subleading t' and t'' hoppings for simplicity, the tight-binding model on the fcc lattice consists of a set of two-dimensional square lattices on xy, yz, and zx planes, respectively, with a rotation by 45° on each plane [Fig. 1(c)]. It has been shown [37] that for a square lattice the CDF is maximally enhanced (suppressed) for $\theta = 0^\circ$ ($\theta = 45^\circ$), which implies for the present case that the CDF is enhanced (suppressed) for $\theta = 45^\circ$ ($\theta = 0^\circ$). The result in Figs. 2(c) and 2(d) indicates that the corrections due to t' and t'' do not significantly change the polarization dependence.

TABLE I. The polarization dependence of the THG susceptibility $\chi(\omega)$ relevant to the resonance at $2\omega = 2\Delta$ for the CDF and Higgs-mode contributions. The polarization-independent functions $A(\omega)$, $B(\omega)$, and $C(\omega)$ are defined in [46].

	$\boldsymbol{e}^I = \boldsymbol{e}^O = \boldsymbol{e}_\theta$	$\boldsymbol{e}^I = \boldsymbol{e}_\theta,\ \boldsymbol{e}^O = \boldsymbol{e}_{\theta+90^\circ}$
CDF	$A(\omega) + 2B(\omega)\sin^2 2\theta$	$B(\omega)\sin 4\theta$
Higgs	$C(\omega)$	0

A general form for the polarization dependence of the CDF and Higgs contributions to the THG susceptibility $\chi(\omega)$ is given in Table I. One can see that the CDF contribution is nonvanishing when $\boldsymbol{e}^O$ is perpendicular to $\boldsymbol{e}^I$. For a general band dispersion, $A(\omega)$ and $B(\omega)$ in Table I have similar orders of magnitude. This means that if the CDF contribution is dominant, the THG should also be observed for the direction perpendicular to the polarization of the incident light. This sharply contrasts with the Higgs-mode contribution, which arises only in the direction parallel to the polarization of the incident light and does not depend on θ. This can be generally understood by the symmetry argument [46] based on the fact that the s-wave pairing is isotropic in the momentum and orbital spaces.

Experimental analysis. We measured the dependence of THG on the electric field polarization with respect to lattice axes. The sample is a NbN thin film on a MgO substrate [47] with $T_c = 15\,\text{K}$. From x-ray scattering we confirmed that the single-crystal (100) NbN is epitaxially grown on (100) MgO with a cube-on-cube in-plane alignment [46]. Figure 3(a) shows a schematic experimental setup for polarization-resolved THz transmission spectroscopy. Strong monocycle THz pulses with vertical polarization ($\| x$ or 0°) were generated by optical rectification in a $LiNbO_3$ crystal with the tilted-pulse-front scheme [48–50]. Bandpass filters were placed to make narrow-band THz pulses with the center frequency of $\omega = 0.5\,\text{THz}$. In front of the sample we set two wire-grid polarizers WGP1 and WGP2, whose respective angles, θ_1 and θ_2, determine the field strength as factored by $\cos\theta_1 \cos(\theta_2 - \theta_1)$. The electric field polarization on the sample is determined solely by θ_2. Angles $\theta_2 = 0^\circ$ and 45° correspond to [100] and [110] directions, respectively, as indicated in the inset of Fig. 3(a). Additional two polarizers WGP3 and WGP4 are placed behind the sample with angles θ_3 and θ_4, respectively. The WGP3 is set to $\theta_3 = \theta_2$ or $\theta_2 + 90^\circ$ for detection of the THG polarized parallel or perpendicular to the incident field, respectively. The extinction ratio for this set up was evaluated as $\sim 10^{-4}$ in the frequency range below $3\omega = 1.5\,\text{THz}$ [46], which is good enough for resolving the polarization state of THG. Transmitted THz pulses were detected by the electro-optic (EO) sampling with a (100) ZnTe crystal.

We first examine the nonlinear transmission spectra in the case of $\theta_2 = 22.5^\circ$, where the CDF should give rise to the THG polarized perpendicular to the incident field according to Table I. Here we set $\theta_4 = \theta_2 + 45^\circ$ so that the transmitted electric field parallel ($\theta_3 = \theta_2$) or perpendicular ($\theta_3 = \theta_2 + 90^\circ$) to the incident field can be directly compared because both are detected with the same projection of 45°

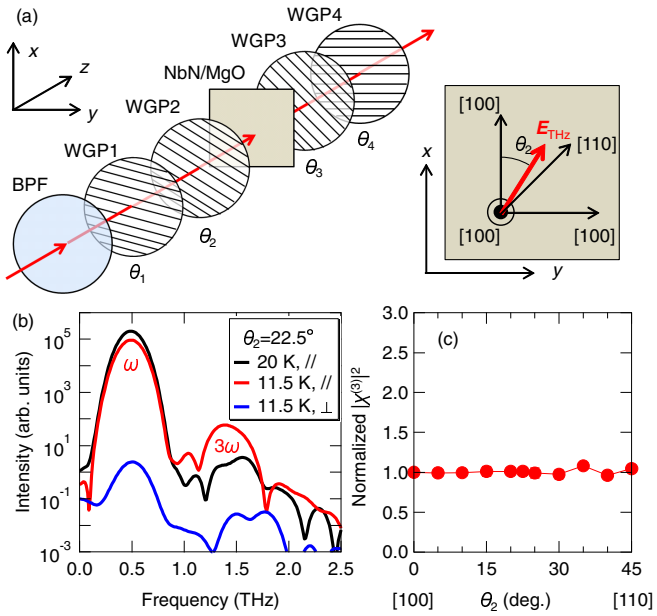

FIG. 3. (a) A schematic experimental setup for THz transmission spectroscopy. WGP: wire-grid polarizer, BPF: bandpass filter. Inset shows the electric field polarization along the crystal axis on the sample surface. (b) Experimental result for the power spectra of the transmitted THz pulse with $\theta_2 = 22.5°$. The black curve is obtained above T_c. Red and blue curves show the data at $2\omega = 2\Delta(T)$ for polarizations parallel and perpendicular to the incident field, respectively. (c) Squared nonlinear susceptibility $|\chi|^2$, normalized at $\theta_2 = 0°$, as a function of the incident polarization angle θ_2.

on the WGP4. Figure 3(b) shows the power spectra of the transmitted pulse with the peak electric field of $E_{THz} \approx 5\,kV/cm$. The black curve shows the data above T_c. The red and blue curves correspond to the parallel and perpendicular configurations, respectively, at $T = 11.5\,K < T_c$, at which $2\omega = 2\Delta(T)$ is satisfied. For the parallel configuration THG is clearly observed at $3\omega = 1.5\,THz$, in a stark contrast to the perpendicular configuration where no THG signal was identified. For other incident polarization angles we observe no THG signals for the perpendicular configuration, either. The THG component parallel to the incident polarization is at least 10^3 times larger than the perpendicular one in the present result, which means that $|B(\omega)|$ in Table I is much smaller than $\max\{|A(\omega)|, |C(\omega)|\}$.

We also investigate the dependence of the THG intensity on the incident field polarization direction by rotating θ_2 from 0° to 45°. For each θ_2, WGP1 is tuned so as to fix $\cos\theta_1 \cos(\theta_2 - \theta_1) = 0.85$, hence a constant field strength. WGP3 is also rotated as $\theta_3 = \theta_2$ to detect the THG polarized parallel to the incident field. WGP4 is fixed at $\theta_4 = 45°$ to maintain the field polarization detected by the EO sampling. From the power spectra we obtained the observed THG intensity $I_{3\omega}^{obs}$ and the observed fundamental intensity I_{ω}^{obs}. Note that the observed values of $I_{3\omega}^{obs}$ and I_{ω}^{obs} are related with the generated THG intensity $I_{3\omega}(\theta_2, E_{THz})$ and the transmitted fundamental intensity $I_{\omega}(\theta_2, E_{THz})$, respectively, by a factor of $\cos^2(\theta_2\text{-}45°)$ because of the projection on the WGP4. Thus we focused on the ratio $R(\theta_2) = I_{3\omega}^{obs}/I_{\omega}^{obs} = I_{3\omega}(\theta_2, E_{THz})/I_{\omega}(\theta_2, E_{THz})$ to cancel out the projection factor. $R(\theta_2)$ is then proportional to $|\chi(\theta_2)|^2|E_{THz}|^4$, where $\chi(\theta_2)$ is the third-order nonlinear susceptibility. We also checked the field strength E_{THz} during the rotation of the WGPs, and confirmed that fluctuation of E_{THz} is negligibly small [46]. Then we obtained the squared nonlinear susceptibility $|\chi(\theta_2)|^2 \propto R(\theta_2)/|E_{THz}(\theta_2)|^4$, as displayed in Fig. 3(c) where the data is normalized at $\theta_2 = 0°$. The THG intensity is seen to be basically constant, changing only within $5 \pm 6\%$ from [100] to [110] directions, namely, the THG intensity hardly depends on the incident field polarization with respect to the crystal axis. Since the polarization-angle dependence of THG arises only from $B(\omega)$ in Table I, the experimental result in Fig. 3(c) elucidates that $|B(\omega)|$ is much smaller than $\max\{|A(\omega)|, |C(\omega)|\}$, which is consistent with the experimental result in Fig. 3(b).

Because the calculations in Figs. 2(c) and 2(d) indicate that $|A(\omega)|$ and $|B(\omega)|$ are of the same order of magnitude, we can conclude that $|C(\omega)| \gg |A(\omega)|$, which means that the contribution of Higgs mode to the THG is much larger than the CDF. This is intriguing, since the result for the relative magnitudes of the two contributions is opposite to the BCS prediction [37]. A possible mechanism for the dominance of the Higgs-mode contribution is that the THG process beyond the BCS approximation contains the retardation effect that significantly enhances the contribution of the resonant THG diagram in strongly electron-phonon-coupled superconductors [38]. Especially, the relative contribution of the Higgs mode is expected to significantly increase when lower-frequency phonons are involved in the paring interaction [38,46]. By taking account of the relationship between the THG and Raman process, where the latter probes the imaginary part of the third-order susceptibility [51], our results imply that the resonant diagrams may play a non-negligible role also in the Raman process in systems with strong retardation effects [52].

Summary. We have studied the polarization dependence of the THG in a superconductor NbN theoretically and experimentally, and revealed that the Higgs mode gives a dominant contribution to the THG far exceeding the CDF contribution. The results also demonstrate that the polarization-resolved nonlinear THz spectroscopy provides a new pathway for investigating collective modes in superconductors. An important future problem is to extend the present scheme to unconventional superconductors such as the high-T_c cuprates.

We wish to thank Y. Gallais for illuminating discussions. This work was supported in part by JSPS KAKENHI (Grants No. JP15H05452, No. JP15H02102, No. JP26247057, and No. JP16K17729), by the Photon Frontier Network Program from MEXT, Japan, by JST PRESTO (Grant No. JPMJPR16PA), and by the ImPACT Program of Council for Science, Technology and Innovation, Cabinet Office, Government of Japan (Grant No. 2015-PM12-05-01) from JST.

[1] D. Pekker and C. M. Varma, Annu. Rev. Condens. Matter Phys. **6**, 269 (2015).

[2] G. E. Volovik and M. A. Zubkov, J. Low Temp. Phys. **175**, 486 (2014).

[3] J. Demsar, K. Biljaković, and D. Mihailovic, Phys. Rev. Lett. **83**, 800 (1999).
[4] R. Yusupov, T. Mertelj, V. V. Kabanov, S. Brazovskii, P. Kusar, J.-H. Chu, I. R. Fisher, and D. Mihailovic, Nat. Phys. **6**, 681 (2010).
[5] T. Mertelj, P. Kusar, V. V. Kabanov, P. Giraldo-Gallo, I. R. Fisher, and D. Mihailovic, Phys. Rev. Lett. **110**, 156401 (2013).
[6] D. Werdehausen, T. Takayama, M. Höppner, G. Albrecht, A. W. Rost, Y. Lu, D. Manske, H. Takagi, and S. Kaiser, arXiv:1611.01053.
[7] Ch. Rüegg, B. Normand, M. Matsumoto, A. Furrer, D. F. McMorrow, K. W. Krämer, H.-U. Güdel, S. N. Gvasaliya, H. Mutka, and M. Boehm, Phys. Rev. Lett. **100**, 205701 (2008).
[8] U. Bissbort, S. Götze, Y. Li, J. Heinze, J. S. Krauser, M. Weinberg, C. Becker, K. Sengstock, and W. Hofstetter, Phys. Rev. Lett. **106**, 205303 (2011).
[9] M. Endres, T. Fukuhara, D. Pekker, M. Cheneau, P. Schau, C. Gross, E. Demler, S. Kuhr, and I. Bloch, Nature (London) **487**, 454 (2012).
[10] P. Merchant, B. Normand, K. W. Krämer, M. Boehm, D. F. McMorrow, and Ch. Rüegg, Nat. Phys. **10**, 373 (2014).
[11] P. W. Anderson, Phys. Rev. **130**, 439 (1963).
[12] P. W. Higgs, Phys. Lett. **12**, 132 (1964).
[13] R. Sooryakumar and M. V. Klein, Phys. Rev. Lett. **45**, 660 (1980).
[14] P. B. Littlewood and C. M. Varma, Phys. Rev. Lett. **47**, 811 (1981).
[15] P. B. Littlewood and C. M. Varma, Phys. Rev. B **26**, 4883 (1982).
[16] M. A. Méasson, Y. Gallais, M. Cazayous, B. Clair, P. Rodière, L. Cario, and A. Sacuto, Phys. Rev. B **89**, 060503 (2014).
[17] T. Cea and L. Benfatto, Phys. Rev. B **90**, 224515 (2014).
[18] R. Matsunaga, Y. I. Hamada, K. Makise, Y. Uzawa, H. Terai, Z. Wang, and R. Shimano, Phys. Rev. Lett. **111**, 057002 (2013).
[19] R. Matsunaga, N. Tsuji, H. Fujita, A. Sugioka, K. Makise, Y. Uzawa, H. Terai, Z. Wang, H. Aoki, and Ryo Shimano, Science **345**, 1145 (2014).
[20] For a review, see e.g., R. Matsunaga and R. Shimano, Phys. Scr. **92**, 024003 (2017).
[21] A possibility of the linear coupling was proposed recently under flow of superfluid condensates: A. Moor, A. F. Volkov, and K. B. Efetov, Phys. Rev. Lett. **118**, 047001 (2017).
[22] A. F. Volkov and S. M. Kogan, Zh. Eksp. Teor. Fiz. **65**, 2038 (1973) [Sov. Phys. JETP **38**, 1018 (1974)].
[23] I. O. Kulik, O. Entin-Wohlman, and R. Orbach, J. Low Temp. Phys. **43**, 591 (1981).
[24] R. A. Barankov, L. S. Levitov, and B. Z. Spivak, Phys. Rev. Lett. **93**, 160401 (2004).
[25] R. A. Barankov and L. S. Levitov, Phys. Rev. Lett. **96**, 230403 (2006).
[26] E. A. Yuzbashyan and M. Dzero, Phys. Rev. Lett. **96**, 230404 (2006).
[27] T. Papenkort, V. M. Axt, and T. Kuhn, Phys. Rev. B **76**, 224522 (2007).
[28] A. P. Schnyder, D. Manske, and A. Avella, Phys. Rev. B **84**, 214513 (2011).
[29] X. Xi and G. L. Carr, Supercond. Sci. Technol. **26**, 114001 (2013).
[30] N. Tsuji and H. Aoki, Phys. Rev. B **92**, 064508 (2015).
[31] A. Akbari, A. P. Schnyder, D. Manske, and I. Eremin, Europhys. Lett. **101**, 17002 (2013).
[32] H. Krull, N. Bittner, G. S. Uhrig, D. Manske, and A. P. Schnyder, Nat. Commun. **7**, 11921 (2016).
[33] T. Cea and L. Benfatto, Phys. Rev. B **94**, 064512 (2016).
[34] Y. Murotani, N. Tsuji, and H. Aoki, Phys. Rev. B **95**, 104503 (2017).
[35] Y. Barlas and C. M. Varma, Phys. Rev. B **87**, 054503 (2013).
[36] T. P. Devereaux and R. Hackl, Rev. Mod. Phys. **79**, 175 (2007).
[37] T. Cea, C. Castellani, and L. Benfatto, Phys. Rev. B **93**, 180507 (2016).
[38] N. Tsuji, Y. Murakami, and H. Aoki, Phys. Rev. B **94**, 224519 (2016).
[39] K. E. Kihlstrom, R. W. Simon, and S. A. Wolf, Phys. Rev. B **32**, 1843 (1985).
[40] S. D. Brorson, A. Kazeroonian, J. S. Moodera, D. W. Face, T. K. Cheng, E. P. Ippen, M. S. Dresselhaus, and G. Dresselhaus, Phys. Rev. Lett. **64**, 2172 (1990).
[41] S. P. Chockalingam, M. Chand, J. Jesudasan, V. Tripathi, and P. Raychaudhuri, Phys. Rev. B **77**, 214503 (2008).
[42] P. Blaha, S. Karlheinz, M. Georg, K. Dieter, and L. Joachim, *WIEN2K* (Karlheinz Schwarz, Technische Universität Wien, Austria, 2001).
[43] L. F. Mattheiss, Phys. Rev. B **5**, 315 (1972).
[44] C. Y. Fong and M. L. Cohen, Phys. Rev. B **6**, 3633 (1972).
[45] T. Amriou, B. Bouhafs, H. Aourag, B. Khelifa, S. Bresson, and C. Mathieu, Physica B **325**, 46 (2003).
[46] See Supplemental Material at http://link.aps.org/supplemental/10.1103/PhysRevB.96.020505 for details of the calculation, sample characterization, polarization resolution, and analysis.
[47] Z. Wang, A. Kawakami, Y. Uzawa, and B. Komiyama, J. Appl. Phys. **79**, 7837 (1996).
[48] J. Hebling, G. Almási, I. Z. Kozma, and J. Kuhl, Opt. Express **10**, 1161 (2002).
[49] J. Hebling, K.-L. Yeh, M. C. Hoffmann, B. Bartal, and K. A. Nelson, J. Opt. Soc. Am. B **25**, B6 (2008).
[50] R. Shimano, S. Watanabe, and R. Matsunaga, J. Infrared, Millimeter, Terahertz Waves **33**, 861 (2012).
[51] Y. R. Shen, *The Principles of Nonlinear Optics* (Wiley, New York, 1984).
[52] A. Kawabata, J. Phys. Soc. Jpn. **30**, 68 (1971).